Aeolian Research 48 (2021) 100653

Contents lists available at ScienceDirect

Aeolian Research

journal homepage: www.elsevier.com/locate/aeolia

Scaling sediment mobilization beneath rotorcraft for Titan and Mars

Jason Rabinovitch [a,*], Ralph Lorenz [b], Eric Slimko [a], Kon-Sheng C. Wang [a]

[a] Jet Propulsion Laboratory, California Institute of Technology, 4800 Oak Grove Drive, Pasadena, CA 91109, USA
[b] Johns Hopkins Applied Physics Laboratory, Laurel, MD 20723, USA

ARTICLE INFO

Keywords:
Rotorcraft
Helicopter
Saltation
Mars Helicopter
Dragonfly
Mars
Titan

ABSTRACT

Using rotorcraft to explore extraterrestrial bodies will allow future missions to explore terrain that is inaccessible to traditional lander/rover missions, and will enable spacecraft to explore much larger distances than previous missions. The upcoming Mars 2020 Rover mission will include the Mars Helicopter (named Ingenuity), a small (< 2 kg) counter-rotating co-axial vehicle, which, if successful, will be the first rotorcraft to fly on a non-terrestrial body. The Dragonfly mission, recently selected through the NASA New Frontier's program, is expected to fly a much larger vehicle on Titan (~ 750 kg) arriving in the early 2030s. On Earth it is commonly observed that both sub-scale and full-scale rotorcraft can mobilize sediment, to varying degrees of magnitude, when a vehicle is operating over regolith. In order to determine the feasibility of performing sediment mobilization experiments (e.g. saltation investigations) beneath a rotorcraft through intentional sediment mobilization (due to the wake produced by the rotating rotors) for future missions, the scaling of aerodynamic and aeolian parameters should be accounted for. Furthermore, in an extreme case, this analysis can also be used as a low-fidelity method to begin to understand any potential risk associated with brownout (large-scale sediment mobilization due to the helicopter rotor wake) to the rotorcraft itself. In this work, a scaling analysis is presented that allows a vehicle designer to quickly investigate the magnitude of sediment mobilization beneath a rotorcraft, without requiring detailed CFD simulations. The analysis confirms that the upcoming Mars Helicopter and Dragonfly missions could be used for sediment mobilization experiments.

1. Introduction

When a rotorcraft is hovering over a loose sediment bed, the interaction between the rotorcraft wake and surface can allow solid particles to be mobilized. Classic sedimentology processes, such as creep and saltation have been observed beneath helicopters operating over sediment beds on the Earth. In addition, other rotorcraft specific phenomena such as particle/vortex interactions and, in extreme cases, particle bombardment beneath the rotor (resulting from particles entrained in the rotor wake) can occur. Such effects have been discussed in previous works, including (Iversen et al., 1982; Milluzzo et al., 2010 and Johnson et al., 2010). When this effect is severe, it is possible for the rotorcraft wake to generate a self-sustaining dust cloud, which in turn can create a visually degraded environment around the helicopter. This severe environment is often referred to as helicopter brownout (while brownout can also refer to electrical function loss due to bus voltage drop in the presence of a short circuit, in this work only the rotorcraft specific brownout caused by massive sediment mobilization is addressed) and has been a subject of study in numerous works (e.g. Milluzzo et al., 2010; Johnson et al., 2010; Jasion and Shrimpton, 2012; Kuhn, 1959; Phillips and Brown, 2009; Wadcock et al., 2008).

Sediment mobilization beneath landers using powered descent has been observed extensively in the past, and was even a topic of great interest during the Apollo era (e.g. Roberts, 1966). During the landing of the Curiosity rover on Mars in 2012, error that was measured from the Terminal Descent Radar is attributed to the radar's line of site interacting with sediment moving on the surface of Mars, which was caused by the high-velocity exhaust exiting the landing engines (Chen et al., 2014). For rotorcraft, like any spacecraft taking off or landing on an unprepared surface, it is important to have an estimate of the expected level of sediment mobilization in order to ensure that all vehicle systems and sensors will be able to operate nominally. Recent advances in numerical approaches for modeling helicopter induced sediment mobilization have increased the fidelity of predictive simulation capabilities, but work remains to reduce errors in even state of the art simulations (Syal, 2012) and to validate predictions against experimental data to quantify uncertainties. High-fidelity simulations may also not be feasible if there is a desire to investigate a large design space of possible vehicle parameters.

* Corresponding author.
E-mail addresses: Jason.Rabinovitch@jpl.nasa.gov, jrabinov@stevens.edu (J. Rabinovitch).

https://doi.org/10.1016/j.aeolia.2020.100653
Received 13 August 2020; Received in revised form 4 November 2020; Accepted 17 November 2020
Available online 7 December 2020

Nomenclature

α_L	Lamb's constant, 1.25643
Γ_v	tip-vortex circulation (m^2/s)
μ	dynamic viscosity (Pa s)
ν	kinematic viscosity (m^2/s)
Ω	rotor angular velocity (rad/s)
ρ	density (kg/m^3)
σ	rotor solidity
τ	shear stress (Pa)
A	rotor area (m^2)
c	chord length (m)
C_T	rotor thrust coefficient
D	rotor diameter (m)
d	vertical distance from the rotor plane to the ground plane (m)
d_p	particle diameter (m)
h_{rotor}	rotor-plane height (m)
R	rotor radius (m)
r_c	vortex-core radius (m)
T	rotor thrust (N)
U	velocity (m/s)
u_*	friction velocity, $\sqrt{\frac{\tau_w}{\rho}}$ (m/s)
v_{LO}	Lamb-Oseen vortex model induced velocity (m/s)
v_{vortex}	tip-vortex induced velocity (m/s)
w	rotor downwash velocity (m/s)
AR	blade aspect ratio (c/R)
RPM	rotations per minute

Furthermore, intentional sediment mobilization beneath a rotorcraft may in fact be desirable in order to perform controlled aeolian experiments on other worlds, which could contribute greatly to understanding aeolian processes for different bodies. Aeolian landforms have been used to attempt to diagnose paleoclimate conditions on both Mars and Titan (e.g. McDonald et al., 2016; Lorenz, 2020b), and critical in these interpretations is an estimate of the threshold wind stress required for the onset of particle movement. There is furthermore an apparent paradox in that stress from freestream winds alone seems generally inadequate to cause dust-lifting on Mars (e.g. Neakrase et al., 2016), requiring other effects such as aggregate breakup, sand abrasion, or backventing (the 'Delta-P effect).

Laboratory tests such as wind tunnel experiments on Earth cannot fully replicate the conditions on other worlds: while attempts may be made, e.g. the substitution of low-density walnut shells for silicate sand on Mars, in order to match the drag to weight ratio (as in Greeley's pioneering experiments in Greeley et al. (1980)), this then changes the particle inertia, which is important for the impact threshold effect. Not all of the non-terrestrial properties can be matched with laboratory experiments, making in situ observations essential. The rare opportunity to directly apply a known wind stress field to a real planetary surface and possibly observe particle transport effects is therefore valuable, and investigating the feasibility of performing these experiments with future rotorcraft is necessary.

The goal of this work is to extend helicopter sediment mobility analysis for a rotorcraft operating near the surface of Mars or Titan, then determine the feasibility of performing aeolian experiments with rotorcraft on other planetary bodies. Specifically, a simplified low-fidelity model will be presented which can be used to quickly determine if sediment mobilization experiments will be feasible beneath a specific rotorcraft vehicle design. While the possibility of brownout for rotorcraft on Mars has been mentioned previously (Young et al., 2005), no detailed analysis has been performed to quantify the possible effects of this phenomena for specific vehicle designs. The predicted magnitude of rotor induced sediment mobilization will also be investigated in this work for both the Mars Helicopter and for Dragonfly (Lorenz, 2017).

2. Mars helicopter and dragonfly rotorcraft designs

Mission concepts to send autonomous flying vehicles to Mars and Titan have been investigated through multiple studies in recent decades (see Young et al., 2005; Colozza, 2002; Colozza, 2003; Lorenz, 2001; Lorenz et al., 2018). These vehicles could contribute to a variety of missions by providing aerial images of the surface at a scale between that which a rover and an orbiting asset can provide, or by adding a mobility capability that can significantly extend the range that a typical rover is expected to cover in its lifetime. If vehicles have a large enough lifting capacity for scientific payloads, then a rotorcraft can even be a stand-alone mission. On bodies like Titan, where gravity is significantly lower than Earth but ambient density is higher, the environment is conducive to exploration with powered aerial vehicles.

The Mars Helicopter (Balaram et al., 2018) will travel to Mars with the Mars 2020 rover mission, which launched on July 30, 2020 (https://mars.nasa.gov/mars2020/). There are strict mass and size constraints for the helicopter in order for it to both interface with the Mars 2020 rover, and to be able to generate enough lift to fly in the low density Martian environment (Fig. 1). In order to try and maximize lift for a given vehicle volume, a counter-rotating coaxial helicopter design was chosen. On the other hand, Dragonfly, which is a stand-alone vehicle to explore Titan, did not have to accommodate as severe size restrictions. The Dragonfly vehicle uses a dual-quadcopter or X-8 layout, which means that the vehicle has a top and bottom motor/rotor at each corner of the vehicle for eight rotors in total (Lorenz et al., 2018). It is expected to launch in the mid-2020s and arrive at Titan in the mid-2030s. As it is a full New Frontiers class mission on its own, the vehicle is significantly

Fig. 1. Artists rendition of both the Mars Helicopter (https://mars.nasa.gov/technology/helicopter/) (top) and Dragonfly (https://dragonfly.jhuapl.edu/) (bottom). Images are not to scale: the rotor diameter for the Mars Helictoper is ~ 1.2 m, while each rotor has an expected diameter of ~ 1.4 m for Dragonfly. The full Dragonfly vehicle mass is expected to be ~ 750 kg, while the Mars Helicopter vehicle mass is ~ 1.8 kg.

larger than the Mars Helicopter (Fig. 1).

Only basic (and approximate) information about the proposed helicopter designs are needed for the analysis performed in the following sections, and vehicle parameters are summarized in Table 1.

In addition to the design differences between the two vehicles, it is important to understand how differences in Martian and Titan atmospheres, as compared to the Earth, present unique, non-standard operating environments for these rotorcraft. Table 2 shows a comparison of some relevant helicopter operating parameters, along with relevant environmental properties for both Mars and Titan.

On Mars, one of the largest challenges to operating a rotorcraft is the low surface pressure and gas density compared to Earth ambient conditions. The low density atmosphere on Mars means that simply generating controlled, stable flight of an autonomous rotorcraft vehicle is quite challenging. While the lower gravity environment lowers the required amount of thrust, the reduction of gravity by roughly one third on Mars does not compensate for the reduced density of the atmosphere, which is approximately 1% that of the Earth's.

The low density environment causes many of the driving aerodynamic parameters of the Mars Helicopter to be different than those of helicopters operating on the earth. One parameter that is commonly used is the Reynold's Number, which is defined to be $Re = \rho UL/\mu$, where ρ is the gas density, U is the velocity, L is a characteristic length scale, and μ is the dynamic viscosity of the gas. This is commonly written as $Re = UL/\nu$, where ν, the gas kinematic viscosity, is defined to be $\nu = \mu/\rho$. The Reynolds number can be interpreted as the ratio of inertial to viscous forces for a given flow. At the tip of a rotor, the tip Reynolds number can be calculated using the blade tip speed as the velocity, and c, the average blade chord, as the length scale. The low density environment on Mars causes the tip Reynolds number for the Mars Helicopter to be approximately two orders of magnitude lower when compared to that for the same helicopter operating on the Earth.

A second important parameter is the tip Mach number for a helicopter rotor. In general, the Mach number is defined to be the ratio of a velocity of interest to the local speed of sound in a gas. Typical rotorcraft designs will ensure that the blade tip Mach number is less than one, and often a maximum of $\sim 0.7-0.8$ in order to maintain blade performance. Due to the low density environment on Mars, a higher RPM is required to generate lift, which means that the RPM is chosen to be as high as possible while maintaining an acceptable tip Mach number ($\lesssim$0.7).

The large differences in operating parameters between Earth and Mars make it challenging and costly to experimentally test Mars helicopter designs on the Earth under relevant flight conditions. Vacuum chambers can produce the correct density and gas composition, but care must be taken to accurately scale the mass properties of the vehicle to compensate for the higher gravity on Earth. In addition, many low pressure facilities do not allow the introduction of loose sediment into the test chamber, necessitating the use of other methods to investigate the possibility of sediment mobilization. If sediment can be introduced into a low pressure facility, then challenges associated with scaling sediment properties themselves (particle size, density, etc.) is a separate challenge that would be introduced. Finally, existing low-pressure subsonic wind tunnels generally do not have a large enough test sections to test a full-scale vehicle of interest.

Table 1
Overview of Mars Helicopter and Dragonfly rotorcraft designs.

Parameter	Mars Helicopter	Dragonfly[a]
Design	Counter-rotating co-axial	Quad octocopter layout (4× counter-rotating co-axial sets of rotors)
Gross Takeoff Mass (kg)	1.8	750
Blade Diameter, D (m)	~ 1.2	~ 1.4
Blade Chord, c (m)	~ 0.1	~ 0.1
RPM	2800	600
Blade aspect ratio, AR=$D/(2c)$	5	8
No. of Blades[b]	4	4
Height of Rotor Plane (m)	0.4	0.8

[a]Dragonfly vehicle is early in development – values are representative-only, and not finalized. [b]Combines blades on the top and bottom rotor for this simplified analysis.

Table 2
Comparison of operating conditions for the Mars Helicopter and for Dragonfly. Mars atmospheric properties taken from Leovy (2001), and Titan atmospheric properties taken from Lorenz et al. (2018). Characteristic particle densities are taken from Iversen et al. (1982) and Lorenz (2014), for Mars and Titan respectively.

Parameter	Mars Helicopter	Dragonfly
Gravity, g (m/s^2)	3.71	1.35
Characteristic Density, ρ (kg/m^3)	1.2×10^{-2}	5.3
Characteristic Temperature (K)	273	94
Characteristic Dynamic Viscosity, μ (Pa s)	1.4×10^{-5}	6.0×10^{-6}
Atmospheric Composition (volume)	95% CO2 3% N2 2% Ar	95% N2 5% CH4
Tip Reynolds # ($U_{tip}\,c/\nu$)	1.8×10^{4}	3.4×10^{6}
Tip Mach #	0.7	0.2
Characteristic Particle Density (kg/m^3)	3000	1000

On Titan, Dragonfly is expected to operate under a very different regime when compared to both Earth and Mars. Here the increased atmospheric density and reduced gravity (Table 2) of Titan enables Dragonfly to spin its rotors at an RPM value that is comparable to full-scale helicopters on the Earth. The tip Reynolds number is also of the same order of magnitude as full-scale terrestrial helicopters, yet the blade tip Mach number is much lower. Titan density and temperatures can be closely met in some cryogenic wind tunnels on Earth, such as the National Transonic Facility (NTF) at NASA Langley, which does allow for aerodynamic testing to be completed under relevant conditions. Once again, the gravity discrepancies must be accounted for during any Earth testing, and similar issues are encountered if testing with regolith is desired (both from a scaling and test facility standpoint).

The following sections will investigate whether or not Dragonfly and the Mars Helicopter are expected to generate sediment mobilization during takeoff and landing.

3. Sediment mobilization predictions

The majority of brownout studies performed in the past have been under standard Earth atmospheric conditions and have been geared towards full-scale helicopters. Recent work has investigated the effect of different scaling parameters on brownout (Johnson et al., 2010; Milluzzo et al., 2010; Lee et al., 2010), but due to the large parameter space under investigation, this is still an ongoing effort.

Many studies have investigated the threshold friction velocity required for the initiation of saltation under different conditions (e.g. Bagnold, 2012; Greeley and Iversen, 1987; Iversen et al., 1982; Greeley et al., 1976); these studies generally investigate the movement of sediment particles due to a steady wind and a fully developed boundary layer. They define a friction threshold velocity, u_{*t}, to be the minimum friction velocity required over a sediment bed for particles to start moving. The threshold friction velocity is defined to be

$$u_{*t} = \sqrt{\frac{\tau_t}{\rho}}, \tag{1}$$

where τ_t is the threshold shear stress required for a particle to start moving, and ρ is the gas density. Both theoretical and experimental investigations have been performed for conditions on different planets, and theoretical expressions for u_{*t} agree with experimental

measurements under a wide range of conditions. In this work, expressions for friction velocity previously determined in Iversen et al. (1982) and Shao et al. (2000), are used for Mars, Titan, and Earth.

The variation in threshold friction velocity between Earth, Mars, and Titan must be accounted for in any sediment mobilization analysis, as the expected threshold friction velocity for a range of particle sizes is predicted to be a factor of approximately 10 higher on Mars than on the Earth, and ranging from a factor of approximately 2 to 10 lower on Titan than Earth, using the model from Iversen et al. (1982) and assuming a particle density (ρ_p) of 3000 kg/m^3 (Fig. 2). The differences in predicted threshhold friction velocities between the different bodies can be attributed to differences in local ambient density and gravitational forces. Two datasets are included in Fig. 2 for Titan - one with a particle density of 3000 kg/m^3, in order to compare to the Venus, Earth, and Mars datasets, and one with a particle density of 1000 kg/m^3. 1000 kg/m^3 is considered a representative value for Titan sediments (e.g. Lorenz, 2014) being approximately the density of water ice ($\sim$ 900 kg/m^3 at room temperature, $\sim$ 940 kg/m^3 at 90 K), though dissolved salts may increase this value. It is also representative of the many organic solids likely present on Titan, e.g. polycyclic aromatic hydrocarbons (PAHs) such as pyrene and phenanthrene, which have bulk densities of $\sim$ 1150 −1270 kg/m^3, which could be reduced somewhat by porosity effects. For the calculations moving forwards in this work, a particle density of 3000 kg/m^3 is assumed for Mars and Earth scenarios (Iversen et al., 1982), and 1000 kg/m^3 is assumed for Titan. The right axis in Fig. 2 shows an approximation of what the free stream velocity could correspond to for a given friction velocity if a canonical flat plate flow configuration was considered. The approximation of $U \simeq 20u_*$ is taken from Lorenz et al. (2014), where the coefficient of drag for a flat plate is approximated to be between $\sim$ 0.001 and $\sim$ 0.01 (in reality this is a function of Re and roughness). This approximation is shown in order to give some physical intuition into how friction velocity correlates to a simplified free stream velocity.

However, a helicopter wake flow is different from a flat boundary layer flow, which is the configuration generally considered for saltation studies. In order to simplify the analysis with the objective of discerning the predicted magnitude of sediment mobilization (including a desire to not have to perform a high-fidelity prediction of the flowfield), a stagnation point flow model is used. This simplifies the complicated dynamics of a helicopter wake operating in ground effect, and allows the shear stress along the surface to be calculated analytically. Results can also be compared to full-scale and sub-scale Earth helicopters in order to find Earth analogous operating conditions for the Mars Helicopter and Dragonfly.

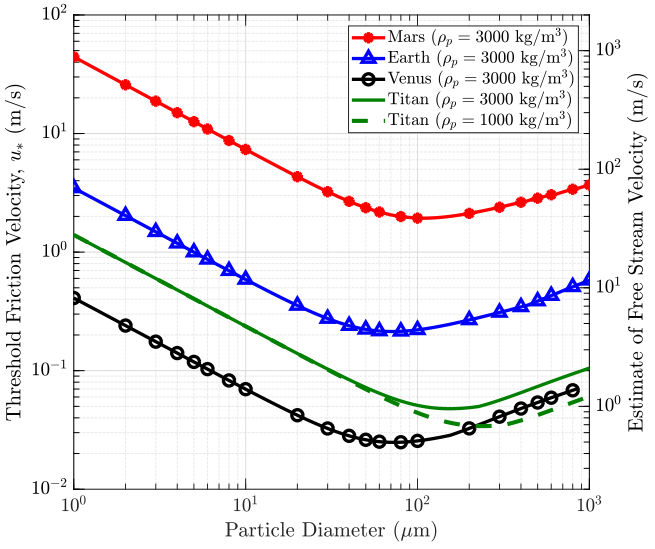

Fig. 2. Variation of threshold friction velocity for saltation using the model provided in Iversen et al. (1982) and assuming a particle density of 3000 kg/m^3 for Venus, Earth, Titan, and Mars, with atmospheric conditions presented in Table 2. A second Titan example is shown with a particle density of 1000 kg/m^3. As particle diameter decreases, interparticle cohesive forces increase, and as particle diameter increases, gravitation forces begin to dominate. This yields a minimum predicted friction threshold velocity at $d_p \approx 100$ μm for $\rho_p = 3000$ kg/m^3 (Iversen et al., 1982; Shao et al., 2000). The right axis shows an approximation of what the free stream velocity could correspond to for a given friction velocity, with the approximation $U \simeq 20u_*$ (Lorenz et al., 2014).

3.1. Stagnation point flow model

A laminar stagnation point flow model is used in order to simplify the wake physics such that analytical calculations can be performed and still give insight into sediment mobilization without having to run high-fidelity CFD simulations. Studies have also shown that the interaction between the blade tip vortices and loose sediment beneath a helicopter can help drive the formation of a brownout dust cloud (Johnson et al., 2010; Perrotta et al., 2015), which suggests that some effect from the tip vortices should be included in the present model. The impinging velocity is modified as a simple approach to including the effect of the tip vortices traveling close to the ground plane. A general schematic of this model is shown in Fig. 3.

The simplicity of this model allows the shear stress generated on the ground beneath a helicopter to be approximated quickly. This shear stress is then compared to the minimum shear stress needed for saltation to occur and is used as an indication as to whether or not sediment mobilization is expected to occur for a given operating condition and at what level of severity.

Hiemenz proposed a similarity solution for planar, laminar, incompressible stagnation point flow, and this solution has been previously extended to include an axisymmetric solution (Schlichting et al., 1960). This solution is a modification to the inviscid axi-symmetric stagnation point solution of $U_r = ar, U_\theta = 0$, and $U_z = -2az$. Here a is a constant representing strain rate of the flow. In order to estimate a in this work, a velocity based on the rotor-induced downwash velocity and tip-vortex induced velocity will be used (see discussion below) along with the distance from rotor plane to the ground (h_{rotor}). Once a is known, the viscous stagnation point velocity distribution and wall shear stress can be calculated. It is assumed that the radius of the impinging jet is infinite in this model.

The rotor-induced downwash in a helicopter wake can be calculated from conservation of momentum arguments (Leishman, 2006). This "impinging jet" will be used as one velocity input for this model. Although the downwash jet from a helicopter will have a diameter smaller than that of its rotor blade diameter, the effect of the infinite diameter jet in this model is assumed to be small when calculating shear stress values on the surface up to one blade radius from the center of the vehicle. The approximate strength of the tip-vortices shed from the rotors can be estimated from the rotorcraft parameters (Milluzzo et al., 2010). The interaction of tip-vortices with the ground below the helicopter is a periodic interaction that cannot be easily accounted for with a steady-state model. As the model proposed in this work is a steady-state model, a characteristic constant vortex velocity is added to the rotor-induced downwash velocity to account for the unsteady tip-vortex induced velocity, and this combined velocity is used as the impinging jet velocity in the calculation of a. This implies that the unsteadiness of tip-vortex impingement on the ground plane beneath the rotorcraft is not accounted for in this work. This model is outlined below, showing the relevant equations used in the calculations.

Following the derivation in Schlichting et al. (1960), it can be shown that the similarity solution for the boundary layer for a viscous axi-symmetric stagnation point flow is

$$\phi''' + 2\phi\phi'' - \phi'^2 + 1 = 0, \tag{2}$$

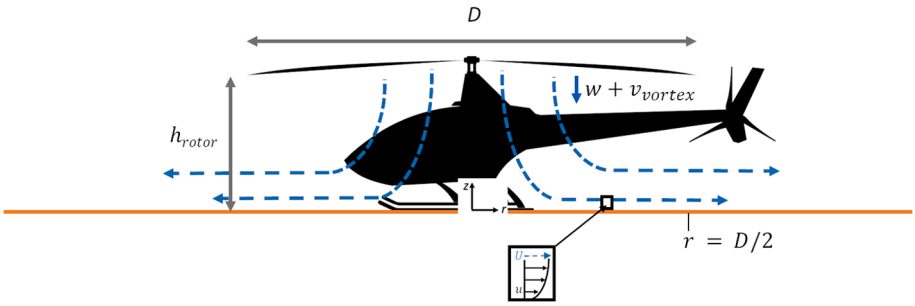

Fig. 3. Schematic of stagnation point flow model used in this work. U represents the radial velocity from the inviscid stagnation point flow model, and u represents the viscous modification to account for the boundary layer growth on the ground.

where ϕ is shorthand for $\phi(\eta)$, and η, the similarity variable, is defined to be $\eta = \sqrt{\frac{a}{\nu}}z$, and $u_r = ar\phi'$. $\phi(\eta)$ is subject to the following boundary conditions: $\phi(0) = 0, \phi'(0) = 0$, and $\phi'(\infty) = 1$. a is defined to be the strain rate of the flow at the stagnation point, which is taken to be $(w + v_{vortex})/(2h_{rotor})$, z is the coordinate perpendicular to the wall, and ν is the kinematic viscosity. From Schlichting et al. (1960), the flow in the radial direction from the stagnation point, u is shown to be $u = ar\phi'$. With these results, the wall shear stress, $\tau_{wall} = \mu\frac{\partial u}{\partial z}|_{z=0}$ is

$$\tau_{wall} = \mu r a^{3/2}\nu^{-1/2}\phi''(0), \tag{3}$$

where μ and ν are the dynamic and kinematic viscosity, respectively, of the atmospheric gas, and r is the radial distance outwards from the center of the jet.

$\phi''(0)$ can be solved numerically from Eq. 2 once and then used for all subsequent calculations using a numerical ordinary differential equation (ODE) boundary value solver (MATLAB *bvp4c* as discussed in Kierzenka and Shampine (2001) is used in this work), and $\phi''(0) \approx 1.31$. μ and ν are properties of the atmosphere, which leaves a and r as unknown quantities. As mentioned previously, Eqs. 2 and 3 are valid assuming an infinite jet impinging on a flat plate. For a helicopter, the jet produced by the rotor downwash will be on the order of the overall rotor blade diameter (D). It is expected that Eq. 3 will not be valid for $r \gg D$, and a value of $\frac{r}{D} = 0.5$ will be used for the rest of this study, which represents a point on the ground beneath the tip of a blade.

From momentum theory, w, the downwash speed, can be shown to be

$$w = 2\sqrt{\frac{T}{2\rho A}}, \tag{4}$$

where T is the thrust generated by the rotor, and A is the area swept by the rotor blades in a full revolution. It is assumed that T is equal to the weight of the helicopter for this analysis, even though during takeoff the thrust is expected to be larger than the weight of the vehicle. Furthermore, this analysis assumes an ideal wake contraction and in the counter-rotating co-axial configurations that both rotors planes are close in height and and can be analyzed using momentum theory.

Simply assuming $a = w/(2h_{rotor})$ does not account for the effect that the rotor tip vortices may have on moving loose sediment below a helicopter. Other works (e.g., Syal, 2012) have modified the threshold friction velocity in order to account for the periodic passages of tip-vortices over the ground surface. A simplified method to account for the tip vortices is to add a component of velocity to w that is associated with a characteristic vortex-induced velocity. In Eq. 3, a is defined to be

$$a = \frac{w + v_{vortex}}{2h_{rotor}}, \tag{5}$$

where v_{vortex} is defined to be (Milluzzo et al., 2010)

$$v_{vortex} = \frac{2.3}{0.1\pi}\frac{T}{\sigma\rho A\Omega D}. \tag{6}$$

Ω is the angular velocity of the rotor blades, and Eq. 6 represents the induced velocity from a line vortex at a point 0.1 c from the vortex center, where c is the blade chord. The empirical constant of 2.3 is included to match experimental observations as discussed in Milluzzo et al. (2010), and $\Gamma_v = 2.3\frac{C_T}{\sigma}(\Omega R)c$, where Γ_v is the tip-vortex circulation, C_T is the rotor thrust coefficient, with $C_T = T/(\rho\pi\Omega^2R^4)$, and σ is the rotor solidity. The factor 2.3 is dependent on the distribution of bound vorticity across the span of the blades. Although, from idealized vortex theory, this constant is equal to 2 while in hover (Milluzzo et al., 2010), this constant is taken to be 2.3 for all blade designs considered in this work for simplicity. This same assumption has been made in other studies (e.g. Milluzzo et al., 2010), and has been shown to better match experimental data. While it is possible to re-write Eqs. 4 and 6 in terms of a variety of different parameters, Eq. 5 can be expanded so that both terms are written in terms of w, as

$$a = (w + \frac{5.75}{\pi}\frac{w^2}{\Omega R\sigma})\Big/(2h_{rotor}). \tag{7}$$

Eq. 5 now represents a velocity whose magnitude contains a component which can be attributed to the steady rotor downwash and the periodic influence of tip-vortices passing over the surface. Eq. 7 can be substituted into Eq. 3 yielding,

$$\tau_{wall} = \frac{\mu r}{(2h_{rotor})^{3/2}}(w + \frac{5.75}{\pi}\frac{w^2}{\Omega R\sigma})^{3/2}\nu^{-1/2}\phi''(0). \tag{8}$$

Results from this model will be shown in Section 3.3. An alternate definition of v_{vortex} was also used, where Eq. 6 was multiplied by the number of rotor blades to account for the possibility of vortex merging (Lee et al., 2010; Milluzzo et al., 2010). The overall results of this analysis were not affected greatly when this additional velocity was included, though the increased jet velocity moved the flow into a compressible regime, further invalidating the use of an incompressible boundary layer similarity solution.

3.2. Tip-vortex decay

In order for a valid comparison to be made between different environments, the expected turbulent/viscous decay of the tip-vortices can be evaluated. A finite amount of time is required for the vortices to be advected towards the surface, and it is assumed that the vortices will be convected downwards at the predicted rotorwash velocity. As outlined in Ramasamy et al. (2007), a modified Lamb-Oseen vortex model is used to approximate the tip-vortex dynamics, where r_c, the vortex core radius is defined to be $r_c = \sqrt{r_o^2 + 4\alpha_L\nu\delta t}$. r_o is the original vortex core radius, α_L is Lamb's constant, which has a value of 1.25643, ν is the gas kinematic viscosity, δ is defined to be $\delta = 1 + a_1\frac{\Gamma_v}{\nu}$, and a_1 is taken to be

6.5×10^{-5} (Ramasamy et al., 2007). The δ term accounts for a non-zero eddy viscosity present inside the tip vortex that causes the vortex core to grow faster through turbulent dissipation than it would if only momentum diffusion through molecular viscosity was included. This modification helps reproduce vortex core growth that has been measured experimentally (Ramasamy et al., 2007). The vortex induced velocity can then be calculated from the standard Lamb-Oseen vortex model as $v_{LO} = \frac{\Gamma_v}{2\pi r}(1 - e^{-r^2/r_c^2})$, where r is the distance from the center of the vortex. The results presented will use the maximum value predicted for v_{LO} for a given point in time. The vortex Reynolds numbers considered in this work as shown in Table 4 range from $\sim 2.5 \times 10^3 - 1.9 \times 10^6$, which are well within the range that this modified Lamb-Oseen vortex model has been used in previous works (Figs. 8,9 from Ramasamy et al. (2007)).

3.3. Results: Comparison to Earth Systems

If the wall shear stress calculated from Eq. 3 is the same order as the theoretically calculated threshold shear stress, then sediment mobilization is expected to occur due to the helicopter wake. However, the severity of this sediment mobilization can also be considered. In order to estimate the magnitude of sediment mobilization, the previously described models are evaluated for existing helicopters of different sizes operating under standard Earth conditions, as well as for the Mars Helicopter and Dragonfly vehicles, operating on Mars and Titan, respectively. For this analysis the mass of the Dragonfly vehicle is divided by 4, in order to assume that each pair of counter-rotating co-axial rotor pairs acts independently (no wake interactions) and that the mass of the vehicle is divided equally.

Table 4 contains a detailed summary of the modeling predictions for sediment mobilization for several different helicopter designs. Both full-scale and model helicopters on Earth are used in this comparison. All helicopter parameters are taken from publicly available sources, and therefore, some values must be estimated. Full-scale helicopter RPMs are chosen to maintain a tip Mach number of 0.7 at sea level and an aspect ratio of 15, if the relevant data was not publicly available.

Before the results of the sediment mobilization model are discussed, Figs. 4 and 5 show comparisons between the predicted vortex evolution for different helicopters and different environments, assuming an initial vortex core size of $0.03c$ (estimate based on Fig. 3 from Ramasamy et al. (2007)). Fig. 4 shows the predicted normalized vortex core growth, while Fig. 5 shows the evolution of the maximum induced velocity, both

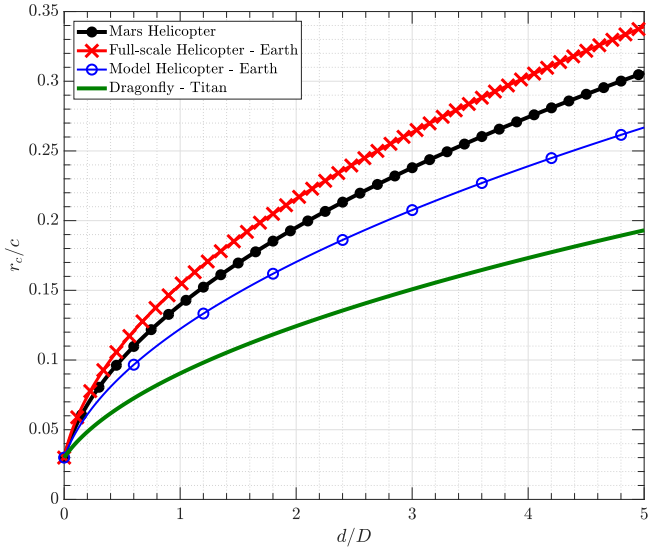

Fig. 4. Normalized evolution of vortex core growth for different vehicles assuming that the tip-vortices convect at the rotor-induced velocity value.

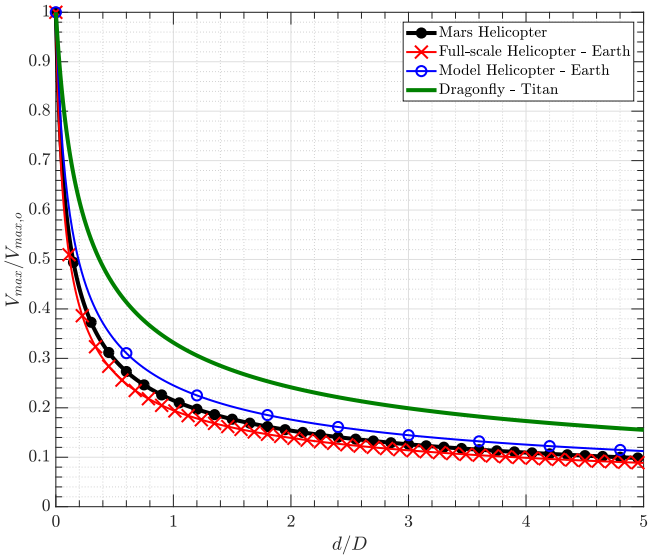

Fig. 5. Normalized evolution of tip-vortex induced velocity for different environments, assuming that the tip-vortices convect at with the rotor-induced velocity.

based on the model described in Section 3.2.

It can be seen that the predicted vortex decay for Dragonfly is not as strong as the other environments/vehicles considered. However, it should be noted that the data is normalized by the assumed convective velocity and the rotor diameter. Not all rotor-planes for helicopters are located at the same non-dimensional distance, h_{rotor}/D above the ground. For the helicopters listed in Table 4, h_{rotor}/D ranges from $\sim 0.3 - 0.7$. Higher values of d/D in Figs. 4,5, where d is the vertical distance from the rotor plane to the ground plane, correspond to the helicopter being in flight at a non-zero altitude above the ground.

The vortex induced velocity as a function of distance from the vortex center r and t, with r_c expanded is

$$v_{LO}(r,t) = \frac{\Gamma_v}{2\pi r}\left(1 - e^{-r^2 \Big/ \left(r_o^2 + 4\alpha_L \nu (1 + a_1 \frac{\Gamma_v}{\nu}) t\right)}\right) \tag{9}$$

As discussed in Section 3.2, the expression for the vortex core radius can be expanded to

$$r_c(t) = \sqrt{r_o^2 + 4\alpha_L \nu (1 + a_1 \frac{\Gamma_v}{\nu}) t} \tag{10}$$

$$\frac{r_c(t)}{r_o} = \sqrt{1 + \frac{4\alpha_L \nu (1 + a_1 \frac{\Gamma_v}{\nu}) t}{r_o^2}} \tag{11}$$

with

$$\frac{\partial r_c(t)}{\partial t} = \frac{1}{2} \frac{4\alpha_L \nu (1 + a_1 \frac{\Gamma_v}{\nu})}{r_c(t)}. \tag{12}$$

Eqs. 9,10,11,12 show the competing factors that contribute to the evolution of v_{LO}. The initial length scale (r_o), which is related to c, along with atmospheric properties (ν), and turbulent dissipation ($1 + a_1 \frac{\Gamma_v}{\nu}$), all contribute to whether or not the vortex induced velocity will change significantly as the vortex travels from the rotor plane towards the ground plane.

Once the flow velocities near the surface, and consequently the shear stress environment can be calculated, the next step of this analysis is to assess the magnitude of sediment mobilization, which requires particle size and density to be assumed. The particle diameters chosen for this analysis correspond to particles expected to be close to having the minimum required threshold friction velocity (Fig. 2, $d_p = 100$ μm for

Mars and Earth, and $d_p = 300$ μm for Titan), as well as a particle diameter of 1 μm, which is chosen to represent dust on all bodies. Fig. 6 shows the ratio of $\frac{u_*}{\overline{u_{*t}}}$ on the ground plane as a function of rotor height above the ground plane for the Mars Helicopter, Dragonfly, and a representative model-scale helicopter flown on the Earth. This accounts for the decay in vortex induced velocity as the vortices advect away from the rotorplane, while Tables 3 and 4 do not account for this decrease in vortex induced velocity. Fig. 7 shows the same information as Fig. 6, but also includes data for a full-scale Earth helicopter. The rotor-plane height of each vehicle is used for the minimum value of d, the distance from the ground to the rotor plane in Figs. 6,7. $\overline{u_{*t}}$ is defined to be the average of the friction velocity calculated when using both the models previously mentioned (Iversen et al., 1982; Shao et al., 2000). The trend of decreasing $\frac{u_*}{\overline{u_{*t}}}$ is expected (sediment mobilization decreases as a rotorcraft increases in altitude) for all rotorcraft and has also been noted for Dragonfly in Lorenz (2020a).

It is also recognized that dust emission in general is a complex phenomenon. For example, dust lifting has been observed on Mars and Earth at friction velocities lower than the predicted threshold friction velocity, and the mechanisms invoked to explain these observations include the break-up of more easily-lofted large dust aggregates, the abrasion of dust from the ground by saltation bombardment by more easily-moved sand, and by 'suction' due to pressure fluctuations (e.g. Neakrase et al., 2016). Nonetheless, comparing the predicted friction velocity to the predicted threshold friction velocity (u_*/u_{*t}) is a useful first-order metric, as well as comparing the predicted surface shear stress to threshold shear stress needed for sediment mobilization (τ/τ_t). Some notable observations for both the Mars Helicopter and Dragonfly (Table 3) are highlighted below.

- For both Dragonfly and the Mars Helicopter, $\frac{u_*}{u_{*t}} > 1$ for $d_p = 100$ μm and $d_p = 300$ μm, respectively, but $\frac{u_*}{u_{*t}} < 1$ for $d_p = 1$ μm. This suggests that dust size particles will not be mobilized due to shear stress alone, but some amount of sediment mobilization is expected for larger particles. This is consistent with the intent of Dragonfly to perform aeolian scientific investigations (Lorenz, 2017), and indicates that investigations, if chosen, could be performed by the Mars Helicopter as well.
- For the Mars Helicopter, the magnitude of $\frac{u_*}{u_{*t}}$ is much closer to those of the model Earth helicopters included in the analysis, specifically the Estes Diamondback model, which is a smaller counter-rotating co-axial vehicle. When this vehicle is flown over sand under Earth conditions, only a minor amount of sediment mobilization is observed, and it is primarily in the radial direction.
- The $\frac{u_*}{u_{*t}}$ ratio predicted by this model decreases as the distance from the rotor plane to the ground plane, d, increases. For the Mars Helicopter, this ratio is equal to 1 when the rotor plane is approximately 0.8 m above the ground, which is less than one rotor diameter above the ground. This implies that sediment mobilization beneath the Mars Helicopter is only expected to occur when the helicopter is operating in relatively close proximity to the ground.
- While the wind stress generated by rotorcraft is highly localized (being concentrated in a circle beneath the rotor perimeter where the rotor tip vortices are advected down to the ground), it may be recalled that at Mars the threshold windspeed to sustain saltation (the 'impact threshold') is rather less than that required to initiate it (the 'fluid threshold', e.g. Sullivan and Kok, 2017; Swann et al., 2020). In the former setting, the momentum of saltating grains can splash other grains into motion, in a 'horizontal avalanche' even when the wind stress is too low to launch grains from rest. Since the stress beneath the Mars Helicopters' rotor blades is directed circumferentially and outwards, particles launched by stress exceeding the fluid threshold merely fly away one or two saltation hops and then come to rest. Conceivably, however, in the presence of a brisk wind rotor stress could initiate particle motion which would not otherwise occur. In other words, if the wind is brisk enough to be above the impact threshold, but is lower than the fluid threshold, then no saltation will be naturally occurring. Rotor operation could trigger saltation which would then be sustained downwind. Although helicopter operators would be unlikely to normally attempt flight in winds above the impact threshold, this scenario should be considered from a rover safety perspective, or perhaps as a deliberate experiment with appropriate precautions.
- On Titan, there is a larger discrepancy in calculated threshold friction velocities between the models used in this work (Iversen et al., 1982; Shao et al., 2000) compared to Earth and Mars, though the range of predicted threshold friction velocities on Titan by these models is consistent with the range presented in Lorenz (2014)
- For Dragonfly, the magnitude of $\frac{u_*}{u_{*t}}$ is between that of model-scale and full-scale Earth rotorcraft. While sediment mobilization is expected, the severity is expected to be less than what is seen for some full-scale Earth rotorcraft.
- For all helicopters considered in Table 4 except for one model-scale helicopter, $v_{vortex}/w > 1$, and ranges between $\sim 2-4$ for full-scale Earth vehicles. This indicates that the vortex induced velocity, as considered in this work, provides an important contribution to the shear stress produced at the ground plane.

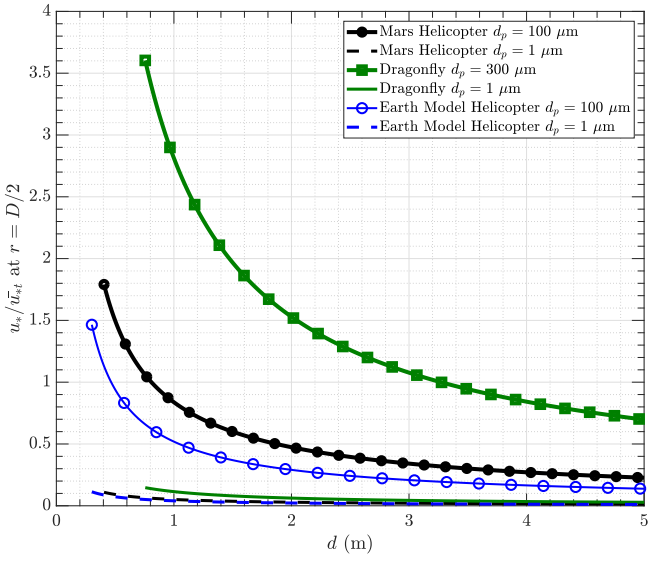

Fig. 6. Evolution of $u_*/\overline{u_{*t}}$ at a radial distance of $D/2$ as a function of vertical distance from the ground to the rotor plane (d).

The results in Table 4 are generally consistent with (Milluzzo et al., 2010), where the authors calculated a normalized wake strength, when this wake strength is normalized by the predicted saltation friction velocity for other environments. It should be noted that some of the complicated phenomena surrounding the physics of a helicopter operating in ground-effect are not captured by this simplified model. For example, the rotor down wash calculated from momentum theory assumes enough space for the velocity to increase from the rotor plane due to the vena contracta effect, and sublteties associated with the spatial evolution of the rotor wake are not captured in this model with the current estimation of the strain rate a. Furthermore, some of the possible complex vortex interactions, especially for counter-rotating rotors, are not accounted for (Kinzel et al., 2019). This analysis does not attempt to account for the re-circulating flow field that must be established for a self-sustaining brownout cloud to be established. Instead, the u_*/u_{*t} ratio is interpreted to represent a severity in terms of sediment mobilization, which could be primarily in the radial direction and/or as a recirculating cloud.

Table 3
Summary of Table 4 highlighting brownout model results.

	Mars Helicopter	Mars Helicopter (Dust)	Dragonfly	Dragonfly (Dust)	Bell UH-1D	Estes Diamondback
v_{vortex}/w	1.3	1.3	1.9	1.9	3.7	2.2
u_*/u_{*t} $(r = D/2)$ (Iversen et al., 1982)	2	0.1	7	0.2	7	2
u_*/u_{*t} $(r = D/2)$ (Shao et al., 2000)	3	0.3	4	0.3	9	3

Table 4
Summary of brownout prediction results.

	Mars		Titan		Earth - Full Scale			Earth - Model Scale		
	Mars Helicopter	Mars Helicopter (Dust)	Dragonfly	Dragonfly (Dust)	CH-53E Super Stallion	AH64A Apache	Bell UH-1D	ALZRC Trex 450 Pro V2	Syma S107	Estes Diamondback
ρ (kg/m^3)	0.012	0.012	5.3	5.3	1.225	1.225	1.225	1.225	1.225	1.225
Temperature (K)	273	273	94	94	298	298	298	298	298	298
Gravity (m/s^2)	3.711	3.711	1.35	1.35	9.81	9.81	9.81	9.81	9.81	9.81
d_p (m)	1.0×10^{-4}	1.0×10^{-6}	3.0×10^{-4}	1.0×10^{-6}	1.0×10^{-4}	1.0×10^{-4}	1.0×10^{-4}	1.0×10^{-4}	1.0×10^{-4}	1.0×10^{-4}
ρ_p (kg/m^3)	3000	3000	1000	1000	3000	3000	3000	3000	3000	3000
ν (m^2/s)	1.2×10^{-3}	1.2×10^{-3}	1.1×10^{-6}	1.1×10^{-6}	1.6×10^{-5}	1.6×10^{-5}	1.6×10^{-5}	1.6×10^{-5}	1.6×10^{-5}	1.6×10^{-5}
Mass (kg)	1.8	1.8	162.5	162.5	33300	10433	4309	0.64	0.034	0.42
D (m)	1.21	1.21	1.4	1.4	24	14.63	14.63	0.71	0.19	0.46
RPM	2800	2800	600	600	190	310	310	1500	3000	1500
AR	5	5	8	8	15	15	15	5	5	8.4
Number of Blades	4	4	4	4	7	4	2	2	4	4
h_{rotor} (m)	0.4	0.4	0.8	0.8	5	4	3	0.2	0.2	0.3
Disk Loading (Pa)	5.81	5.81	142.51	142.51	722.11	608.84	251.46	15.86	11.76	25.10
w (m/s)	31.12	31.12	7.33	7.33	34.34	31.53	20.26	5.09	4.38	6.40
Tip Speed (m/s)	177.40	177.40	43.98	43.98	238.76	237.47	237.47	55.76	29.85	35.91
Chord (m)	0.12	0.12	0.09	0.09	0.80	0.49	0.49	0.07	0.02	0.03
Rotor Solidity	0.25	0.25	0.16	0.16	0.15	0.08	0.04	0.13	0.25	0.15
C_T	0.02	0.02	0.01	0.01	0.01	0.01	0.004	0.004	0.01	0.02
Γ_v (m^2/s)	2.98	2.98	0.77	0.77	30.58	27.66	22.84	0.30	0.06	0.24
v_{vortex} (m/s)	39.23	39.23	14.06	14.06	60.84	90.26	74.56	6.67	4.63	13.78
$C_T/(\sigma)$	0.06	0.06	0.09	0.09	0.07	0.10	0.09	0.03	0.04	0.10
Re_v	2.5×10^3	2.5×10^3	6.8×10^5	6.8×10^5	1.9×10^6	1.7×10^6	1.4×10^6	1.9×10^4	3.5×10^3	1.5×10^4
Tip Re	1.8×10^4	1.8×10^4	3.4×10^6	3.4×10^6	1.2×10^7	7.2×10^6	7.2×10^6	2.5×10^5	3.5×10^4	6.1×10^4
v_{vortex}/w	1.3	1.3	1.9	1.9	1.8	2.9	3.7	1.3	1.1	2.2
u_*/u_{*t} $(r = D/2)$ (Iversen et al., 1982)	2	0.1	7	0.2	6	7	7	2	1	2
u_*/u_{*t} $(r = D/2)$ (Shao et al., 2000)	3	0.3	4	0.3	7	8	9	3	1	3
τ/τ_t $(r = D/2)$ (Iversen et al., 1982)	6	0.01	44	0.03	38	47	49	6	1	5
τ/τ_t $(r = D/2)$ (Shao et al., 2000)	7	0.1	17	0.1	56	69	73	59	2	7

4. Conclusions

This work presents a simplified scaling analysis that can be used as a quick way to investigate the expected magnitude of sediment mobilization for different rotorcraft operating in different environments, with a focus on the upcoming Mars Helicopter and Dragonfly missions. Based on the general vehicle parameters, both missions are expected to cause some sediment mobilization during take-off and landing. This sediment mobilization can be utilized for future aeolian investigations on non-terrestrial bodies. This model, which does not require high-fidelity calculations, accounts for tip-vortex induced velocity in addition to the rotor wash, and investigates how tip-vortex decay is expected to evolve

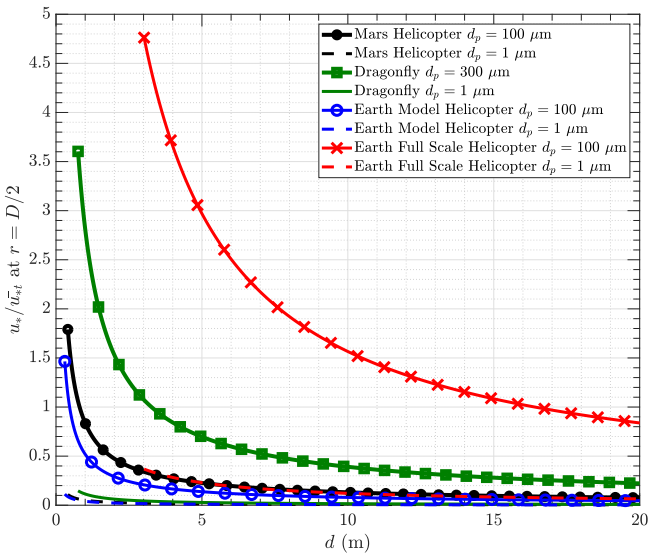

Fig. 7. Evolution of $u_*/\overline{u_{*t}}$ at a radial distance of $D/2$ as a function of vertical distance from the ground to the rotor plane (d), including a full-scale Earth vehicle.

for different vehicles operating in different environments.

CRediT authorship contribution statement

Jason Rabinovitch: Conceptualization, Methodology, Software, Visualization, Writing - original draft, Writing - review & editing. **Ralph Lorenz:** Conceptualization. **Eric Slimko:** Supervision, Conceptualization, Methodology. **Kon-Sheng C. Wang:** Supervision.

Declaration of Competing Interest

The authors declare that they have no known competing financial interests or personal relationships that could have appeared to influence the work reported in this paper.

Acknowledgments

Parts of this research were carried out at the Jet Propulsion Laboratory, California Institute of Technology, under a contract with the National Aeronautics and Space Administration (80NM0018D0004). RL is supported by NASA via contract NNN06AA01C. The authors would like to thank the entire Mars Helicopter and Dragonfly teams.

References

Bagnold, R.A., 2012. The physics of blown sand and desert dunes. Courier Corporation.
Balaram, B., Canham, T., Duncan, C., Grip, H.F., Johnson, W., Maki, J., Quon, A., Stern, R., Zhu, D., 2018. Mars helicopter technology demonstrator. In: AIAA Atmospheric Flight Mechanics Conference. AIAA.
Chen, C.W., Pollard, B.D., 2014. Radar terminal descent sensor performance during mars science laboratory landing. J. Spacecraft Rockets 51 (4), 1208–1216.
Colozza, A.J., 2002. Planetary exploration using biomimetics: An entomopter for flight on mars. In NIAC Fellows Conference, Houston, TX, June 11–12, 2002.
Colozza, A.J., 2003. Comparison of mars aircraft propulsion systems. NASA/CR-2003-212350.
Greeley, R., Iversen, J.D., 1987. Wind as a geological process: on Earth, Mars, Venus and Titan. CUP Archive 4.
Greeley, R., White, B., Leach, R., Iversen, J., Pollack, J., 1976. Mars: Wind friction speeds for particle movement. Geophys. Res. Lett. 3 (8), 417–420. https://doi.org/10.1029/GL003i008p00417.
Greeley, R., Leach, R., White, B., Iversen, J., Pollack, J., 1980. Threshold windspeeds for sand on mars: Wind tunnel simulations. Geophys. Res. Lett. 7 (2), 121–124. https://doi.org/10.1029/GL007i002p00121.
Iversen, J., White, B., 1982. Saltation threshold on earth, mars and venus. Sedimentology 29 (1), 111–119.
Jasion, G., Shrimpton, J., 2012. Prediction of Brownout Inception Beneath a Full-Scale Helicopter Downwash. J. Am. Helicopter Soc. 57 (4), 1–13. https://doi.org/10.4050/JAHS.57.042006. ISSN 21616027.URL: http://www.ingentaconnect.com/content/ahs/jahs/2012/00000057/00000004/art00006.
Johnson, B., Leishman, J.G., Sydney, A., 2010. Investigation of Sediment Entrainment Using Dual-Phase, High-Speed Particle Image Velocimetry. J. Am. Helicopter Soc. 55 (4), 042003 https://doi.org/10.4050/JAHS.55.042003. ISSN 00028711.
Kierzenka, J., Shampine, L.F., 2001. A bvp solver based on residual control and the maltab pse. ACM Trans. Math. Softw. 27 (3), 299–316. https://doi.org/10.1145/502800.502801. ISSN 0098-3500.
Kinzel, M.P., Cornelius, J.K., Schmitz, S., Palacios, J.L., Langelaan, J.W., Adams, D., Lorenz, R., 2019. An investigation of the behavior of a coaxial rotor in descent and ground effect. In: AIAA Scitech 2019 Forum. URL https://arc.aiaa.org/doi/abs/10.2514/6.2019-1098.
Kuhn, R.E., 1959. An investigation to determine conditions under which downwash from vtol aircraft will start surface erosion from various types of terrain. National Aeronautics Space Administration.
Lee, T.E., Leishman, J.G., Ramasamy, M., 2010. Fluid Dynamics of Interacting Blade Tip Vortices with a Ground Plane. J. Am. Helicopter Soc. 55 (2), 022005 https://doi.org/10.4050/JAHS.55.022005. ISSN 00028711. URL: http://www.ingentaconnect.com/content/ahs/jahs/2010/00000055/00000002/art00005.
Leishman, G.J., 2006. Principles of helicopter aerodynamics. Cambridge University Press.
Leovy, C., 2001. Weather and climate on mars. Nature 412 (6843), 245–249.
Lorenz, R.D., 2001. Flight power scaling of airplanes, airships, and helicopters: Application to planetary exploration. J. Aircraft 38 (2), 208–214.
Lorenz, R.D., 2014. Physics of saltation and sand transport on titan: A brief review. Icarus 230, 162–167.
Lorenz, R.D., 2017. In-situ measurement of the saltation threshold of titan's sands with downwash from a rotorcraft lander. In: Fifth International Planetary Dunes Workshop, page Abstract #3043. Lunar and Planetary Institute, Houston.
Lorenz, R.D., 2020a. Triboelectric charging and brownout hazard evaluation for a planetary rotorcraft. In: AIAA AVIATION 2020 FORUM. https://doi.org/10.2514/6.2020-2837.
Lorenz, R.D., 2020b. Martian ripples making a splash. J. Geophys. Res.: Planets 125 (10). https://doi.org/10.1029/2020JE006658. URL: https://agupubs.onlinelibrary.wiley.com/doi/abs/10.1029/2020JE006658.
Lorenz, R.D., Zimbelman, J.R., 2014. Dune worlds: How windblown sand shapes planetary landscapes. Springer Science & Business Media, p. page 46..
Lorenz, R.D., Turtle, E.P., Barnes, J.W., Trainer, M.G., Adams, D.S., Hibbard, K.E., Sheldon, C.Z., Zacny, K., Peplowski, P.N., Lawrence, D.J., et al., 2018. Dragonfly: A rotorcraft lander concept for scientific exploration at titan. Johns Hopkins APL Technical Digest 34 (3), 14.
G.D. McDonald, A.G. Hayes, R.C. Ewing, J.M. Lora, C.E. Newman, T. Tokano, A. Lucas, A. Soto, and G. Chen. Variations in titan's dune orientations as a result of orbital forcing. Icarus, 270: 197–210, 2016. ISSN 0019–1035. doi: 10.1016/j.icarus.2015.11.036. http://www.sciencedirect.com/science/article/pii/S0019103515005643. Titan's Surface and Atmosphere.
Milluzzo, J., Leishman, J.G., 2010. Assessment of rotorcraft brownout severity in terms of rotor design parameters. J. Am. Helicopter Soc. 55 (3), 32009.
Neakrase, L., Balme, M., Esposito, F., Kelling, T., Klose, M., Kok, J., Marticorena, B., Merrison, J., Patel, M., Wurm, G., 2016. Particle lifting processes in dust devils. Space Sci. Rev. 203 (1), 347–376.
Perrotta, G., Glucksman-Glaser, M., Jones, A.R., 2015. Similarity parameters for the characterization of sediment mobilization by unsteady rotor wakes. J. Aircraft 52 (6), 2090–2095. https://doi.org/10.2514/1.C033245.
Phillips, C., Brown, R.E., 2009. Eulerian Simulation of the Fluid Dynamics of Helicopter Brownout. J. Aircraft 46 (4), 1416–1429. https://doi.org/10.2514/1.41999. ISSN 0021-8669.
Ramasamy, M., Leishman, J., 2007. A Reynolds Number Based Blade Tip Vortex Model. J. Am. Helicopter Soc. 214–223.
Roberts, L., 1966. The interaction of a rocket exhaust with the lunar surface(rocket exhaust jet interaction with lunar surface dust layer). Agard Fluid Dyn. Aspects Space Flight 2.
Schlichting, H., et al., 1960. Boundary layer theory, vol. 960. Springer.
Shao, Y., Lu, H., 2000. A simple expression for wind erosion threshold friction velocity. J. Geophys. Res.: Atmospheres 105 (D17), 22437–22443. https://doi.org/10.1029/2000JD900304.
Sullivan, R., Kok, J.F., 2017. Aeolian saltation on mars at low wind speeds. J. Geophys. Res.: Planets 122 (10), 2111–2143. https://doi.org/10.1002/2017JE005275. https://agupubs.onlinelibrary.wiley.com/doi/abs/10.1002/2017JE005275.
Swann, C., Sherman, D.J., Ewing, R.C., 2020. Experimentally derived thresholds for windblown sand on mars. Geophys. Res. Lett. 47 (3), e2019GL084484 https://doi.org/10.1029/2019GL084484.
Syal, M., 2012. Development of a Lagrangian-Lagrangian methodology to predict brownout dust clouds. PhD thesis, University of Maryland, College Park, 2012.
Wadcock, A.J., Ewing, L.A., Solis, E., Potsdam, M., Rajagopalan, G., 2008. Rotorcraft downwash flow field study to understand the aerodynamics of helicopter brownout. Technical report. National Aeronautics and Space Administration Moffett Field CA AMES Research.
Young, L.A., Aiken, E., Lee, P., Briggs, G., 2005. Mars rotorcraft: possibilities, limitations, and implications for human/robotic exploration. In: Aerospace Conference, 2005 IEEE. IEEE, pp. 300–318.